Combined Adjustment of MOC Stereo Imagery and MOLA Altimetry Data

Jong-suk Yoon and Jie Shan

Abstract

Aboard Mars Global Surveyor (MGS), the Mars Orbiter Laser Altimeter (MOLA) collects accurate laser altimetry data over the Martian surface, while the Mars Orbiter Camera (MOC) acquires high resolution images. Recent studies have found that certain systematic misregistration exists among these two types of data due to a number of causes. In this research, a combined adjustment is proposed to correct such misregistration and accurately determine ground positions. Primary participants in this process are MOLA ranges and MOLA ground points, MOC image orientation data, and tie points collected from the MOC Narrow Angle (NA) stereo images. It is shown that the combined adjustment is very beneficial when the trajectory data has a large inconsistency. The outcome is the refined MOC image orientation and refined ground positions, which are validated by the improved MOC and MOLA registration as an independent evaluation. The theoretic study shows the ground position precision of the combined adjustment varies from 28 to 178 meters, depending on the quality of the trajectory data.

Introduction

Mars Global Surveyor (MGS) mission provides accurate and comprehensive mapping data over the Martian surface. Its primary objectives are to collect data about the Martian surface, atmosphere, and magnetic properties, and to build a comprehensive dataset for future mission planning (Albee *et al.*, 2001). Mapping instruments aboard MGS are Mars Orbiter Laser Altimeter (MOLA) and Mars Orbiter Camera (MOC). MOLA (Abshire *et al.*, 2000; Smith *et al.*, 2001) data is considered to be the most accurate mapping data at present with an absolute accuracy of approximately 10 m vertically and approximately 100 m horizontally (Neumann *et al.*, 2001). MOC is a linear pushbroom sensor system (Malin and Edgett, 2001), which provides up to 1.4 m high-resolution panchromatic images from its narrow angle (NA) camera, and 248 m low-resolution multispectral images from its two wide angle (WA) cameras. The objective of this work is to study the combined use of various available mapping data to accurately determine ground positions for precise Mars topographic mapping.

MGS photogrammetric mapping and digital elevation model (DEM) production have been reported recently. Much of the effort is made to identify and measure control points on MOC images based on MOLA profile or MOLA-interpolated DEM, which is used as a control source. Anderson and Parker (2002) align MOC images to MOLA profiles by empirically matching topographic features for Mars Exploration Rover (MER) candidate landing sites. Kirk *et al.* (2002; 2003) use MOC NA images to produce high resolution DEM for the selected MER candidate landing sites. In this process, MOLA generated DEM is used as control. They vary the number of MOC orientation parameters adjusted, depending on whether the MOLA DEM locally contains identifiable features that can be used for horizontal control. If so, the nadir image is adjusted to give horizontal registration to MOLA contours. Elevations sampled from the MOLA DEM are then assigned to all tie points as constraints, and the off-nadir image is adjusted. If the MOLA DEM is featureless, the nadir image is left unadjusted and the second step is performed. Ivanov (2003) generates 10 meter resolution DEM from MOC NA images after the algorithms are validated with MOC WA images. The known camera models are used in this process. It is pointed out that MOC pointing knowledge is very important in this step. This study confirms the previously reported unknown oscillations of the spacecraft. Rosiek *et al.* (2001; 2005) first constrain tie points horizontally to an image mosaic that has been tied to the MOLA DEM, then constrain points vertically to the elevations interpolated from the MOLA DEM at the horizontal locations. The sampling of the MOLA DEM to obtain the elevations is iterated as the solution is refined, to allow for the change in horizontal position. A similar approach is used by Archinal *et al.* (2004) to make the mosaic that Rosiek *et al.* (2001; 2005) start with, except that the horizontal control image is obtained by relief-shading the MOLA DEM. In addition, Caplinger (2003) reports mass DEM production using MOC NA images. A model-based stereo extraction technique is used through parametric sensor adjustments to derive relative height differences from a stereo image pair. A seed DEM produced from gridded MOLA data is used as an initial height estimate to reduce the searching area over which image matching is done. The DEM resolution is typically about 16 meters/pixel. Ebner *et al.* (2004) and Albertz *et al.* (2005) describe an approach where MOLA DEM is used in the bundle adjustment such that the elevations of tie points are constrained to the interpolated surface through the MOLA DEM.

In the photogrammetric evaluation of the MGS mapping data, Shan *et al.* (2005) project a MOLA profile onto the two images of a MOC NA stereo pair. A study over three selected MER candidate landing sites shows that there exits an average of approximately 325 m systematic MOLA and MOC registration offset, which must be corrected for precise topographic mapping. Parker *et al.* (2004) report a approximately 300 m

Geomatics Engineering, School of Civil Engineering, Purdue University, 550 Stadium Mall Dr., West Lafayette, IN 47907-2051 (jshan@ecn.purdue.edu).

Photogrammetric Engineering & Remote Sensing
Vol. 71, No. 10, October 2005, pp. 1179–1186.

0099-1112/05/7110–1179/$3.00/0

location difference of rover Spirit landing site determined by using orbital tracking and MOLA DEM. Subsequently, this paper proposes a combined (bundle) adjustment to correct such misregistration, determine the ground points for MOC photogrammetric mapping and evaluate the performance of the proposed approach. Specifically, the proposed combined adjustment introduces tie points measured on the MOC NA images and includes MOLA range measurements, which have an absolute accuracy better than 10 m (Smith *et al.*, 2001). Other participants in the combined adjustment are MOLA (ground) points determined by MOAL team (Neumann *et al.*, 2001) and MGS trajectory (including both position and pointing) data. Comparing to the methods reviewed above, we will integrate MOLA ranges and MOLA points into the bundle adjustment of MOC NA images. Because MOLA-derived DEM may potentially be subject to the effect of uneven ground spacing of MOLA points in along track (approximately 330 m) and across track (up to kilometers in low latitude regions), MOLA points instead of MOLA-derived DEM are used in this study. Trajectory data and MOLA points provide the reference for the combined adjustment. They and the photogrammetric network will fit with each other within certain tolerance. Presented below are the MGS mapping data, and the models, results, and evaluation of the combined adjustment for three study sites.

MGS Mapping Data Used

The MGS mapping data used in this study includes MOC NA images, MOLA ranges, MOLA points (3D coordinates), and MGS trajectory data. There are an abundance of MOC NA stereo images available as stated in Kirk *et al.* (2004). Table 1 summarizes the main properties of the stereo images used in this study. The stereo geometry of the chosen MOC images is across track configuration: the nadir image from one orbit has a small emission angle, while the off-nadir image from a different orbit has a large emission angle in the across-track direction. All MOC images used in this study belong to the mapping phase Extension 1, except that the right image of Eos Chasma (E04-01275) was taken in the mapping phase Extension 2. The MOLA points used were simultaneously collected from the same orbit as the MOC images. Among several standard MOLA data products, the Precision Experiment Data Record (PEDR) (Slavney and Arvidson, 2000) generated through crossover adjustment (Neumann *et al.*, 2001) is chosen. This study uses the then-latest PEDR Version J files, whereas future study should consider the most up to date version (Version L at the time of writing). Table 1 lists all six MOLA profiles along with their corresponding MOC images. The number of MOLA points in this table refers to the points within the MOC image region.

The MGS trajectory data is extracted using Spacecraft, Planet, Instrument, C matrix (sensor orientation) and Event (SPICE) library (Acton, 1996) provided by the Navigation Ancillary Information Facility (NAIF) of NASA. The navigation data is stored as kernels in binary or text formats, and can be accessed by time. The necessary kernels for the calculation of MOC exterior orientation are the leap seconds kernel (LSK), planetary constants kernel (PCK), spacecraft clock kernel (SCLK), instrument kernel (IK), orientation kernel (CK), and spacecraft position kernel (SPK). The SPK kernel used in this study was produced by the MGS Navigation Team. The above kernels can be accessed from **ftp://naif.jpl.nasa.gov/pub/naif/MGS/kernels/**.

It should be noted that preprocessing must be applied once the above data is acquired. Such preprocessing includes the calculation of the 3D coordinates of MOLA points based on the information in PEDR files, and the conversion of IAU1991 to IAU2000 (Seidelmann *et al.*, 2002; Duxbury *et al.*, 2002) if needed, where the combined adjustment is to be conducted. Besides, verified corrections including CK kernel time bias and MOLA clock bias must also be conducted. For detailed data properties and data preprocessing steps, refer to Shan *et al.* (2005).

Formulation of the Combined Adjustment

The combined adjustment primarily integrates the MOLA ranges, MOLA points, MOC exterior orientation (including both position and pointing), and tie points in the MOC stereo images. The tie points are manually and automatically collected with IMAGINE OrthoBASE® Pro 8.5.1. They will participate in the combined adjustment as measurements (observations). The total number of tie points in each stereo pair is listed in Table 1.

The above different types of data will form observation equations separately in the combined adjustment. For image measurements, they are related to the ground coordinates X_i, Y_i, Z_i and exterior orientation parameters of the j^{th} image through the collinearity equations (Wang, 1990)

$$\begin{aligned} 0 + f_j \frac{m_{11}^{ij}(X_i - X_{ij}^c) + m_{12}^{ij}(Y_i - Y_{ij}^c) + m_{13}^{ij}(Z_i - Z_{ij}^c)}{m_{31}^{ij}(X_i - X_{ij}^c) + m_{32}^{ij}(Y_i - Y_{ij}^c) + m_{33}^{ij}(Z_i - Z_{ij}^c)} &= 0 \\ y_{ij} + f_j \frac{m_{21}^{ij}(X_i - X_{ij}^c) + m_{22}^{ij}(Y_i - Y_{ij}^c) + m_{23}^{ij}(Z_i - Z_{ij}^c)}{m_{31}^{ij}(X_i - X_{ij}^c) + m_{32}^{ij}(Y_i - Y_{ij}^c) + m_{33}^{ij}(Z_i - Z_{ij}^c)} &= 0 \end{aligned} \quad (1)$$

where y_{ij} is the across track image coordinate of the i^{th} point on the j^{th} image; the corresponding along track coordinate has been set to the detector location, which is defined as zero

TABLE 1. PROPERTIES OF MOC AND MOLA DATA

Site Name	Eos Chasma		Gusev Crater		Isidis Planitia	
Image Name	E02-02855	E04-01275	E02-00665	E02-01453	E02-01301	E02-02016
Stereo	Left	Right	Left	Right	Left	Right
Emission Angle (deg.)	0.16	17.97	0.2	22.1	13.0	0.2
B/H Ratio	0.41		0.41		0.24	
Acquisition Time	03/31/01 (18:17:09)	05/18/01 (00:48:12)	03/08/01 (12:52:54)	03/17/01 (18:39:14)	03/15/01 (23:34:57)	03/23/01 (04:17:44)
Exposure Time (ms)	1.8078	1.2052	1.4462	1.4462	0.9642	1.4462
File size (H*W)	9856*672	7424*1024	10112*1024	8960*1024	7680*1024	7680*1024
MOC Pixel Size (m)	5.5	4.1	4.4	4.9	3.3	4.4
MOLA Profile Name	ap19215j	ap19802j	ap18933j	ap19043j	ap19019j	ap19117j
# MOLA Points	174	76	142	124	71	107
MOLA Spacing (m)	305	341	305	341	340	304
# Tie Points	162		154		41	

$X_i,\ Y_i,\ Z_i$	are the ground coordinates of the i^{th} point
$X_{ij}^c,\ Y_{ij}^c,\ Z_{ij}^c$	are the sensor position for the i^{th} point on the j^{th} image
$m_{11}^{ij} \cdots m_{33}^{ij}$	are the elements of the rotation matrix formed by the sensor pointing angles ω_{ij}, φ_{ij}, κ_{ij} (the i^{th} point on the j^{th} image), and
f_j	is the focal length of the j^{th} image

For the sensor position and pointing at i^{th} scan line x_{ij} (the along track coordinate), they are modeled by a second order polynomial:

$$\begin{aligned} X_{ij}^c &= a_{0j} + a_{1j}x_{ij} + a_{2j}x_{ij}^2 & \omega_{ij} &= d_{0j} + d_{1j}x_{ij} + d_{2j}x_{ij}^2 \\ Y_{ij}^c &= b_{0j} + b_{1j}x_{ij} + b_{2j}x_{ij}^2 & \varphi_{ij} &= e_{0j} + e_{1j}x_{ij} + e_{2j}x_{ij}^2 \\ Z_{ij}^c &= c_{0j} + c_{1j}x_{ij} + c_{2j}x_{ij}^2 & \kappa_{ij} &= f_{0j} + f_{1j}x_{ij} + f_{2j}x_{ij}^2 \end{aligned} \quad . \qquad (2)$$

The coefficients in Equation 2 are initially determined by using the SPICE kernels through a sensor modeling process (Shan *et al.*, 2005). First, the entire acquisition time period of a MOC image is equally divided into 30 intervals. The time instants at these intervals are then used as an index to extract and calculate the MOC scan line positions and pointing from the SPICE kernels. For each MOC image, positions and pointing are calculated at these equally spaced time intervals. They will then be used in Equation 2 to determine the polynomial coefficients based on the least squares criterion.

The MOLA ranges are formularized by the Euclidean distance as a function of the sensor position and MOLA point

$$r_k - \sqrt{(X_{kj}^c - X_k)^2 + (Y_{kj}^c - Y_k)^2 + (Z_{kj}^c - Z_k)^2} = 0 \qquad (3)$$

where, r_k is the k^{th} MOLA range, X_{kj}^c, Y_{kj}^c, Z_{kj}^c are the sensor position for the k^{th} MOLA point on the j^{th} image, and X_k, Y_k, Z_k are the ground coordinates of the k^{th} MOLA point.

All the participants in the combined adjustment are divided into two general categories: measurements and weighted parameters. The weighted parameters will form a set of pseudo observation equations in the combined adjustment (Mikhail *et al.*, 2001):

$$pseudo\ observation + correction - parameter = 0. \qquad (4)$$

In our study, all image points and MOLA ranges are treated as measurements, and they will respectively form the observation Equations 1 and 3. While tie points are direct measurements on MOC images, the image coordinates of MOLA points are initially obtained by back projecting the MOLA points onto MOC images as described in (Shan *et al.*, 2005). These initially determined image point locations are not forced to correspond to the MOLA ground positions. Instead, they will be corrected in the combined adjustment such that a consistent set of updated image point locations and exterior orientation parameters satisfies Equations 1, 2, and 3. All ground points and exterior orientation are treated as weighted parameters. The initial ground positions of tie points are obtained through an intersection using the exterior orientation determined from sensor modeling (Shan *et al.*, 2005). For the MOLA points, their initial ground coordinates derived from PEDR files are used as weighted parameters to form Equation 4. Similarly, the coefficients in Equation 2 determined through sensor modeling will form a set of pseudo observation equations based on Equation 4. It should be noted that introducing pseudo observation equations is a quite common treatment in bundle adjustment as documented in (Mikhail *et al.*, 2001; Wang, 1990). It provides the flexibility to properly weigh any participants in the combined adjustment based on *a priori* knowledge about their precision. The adjustment is based on the least squares principle, i.e., the weighted squared sum of the residuals of observations and pseudo observations should be minimized. Since Equations 1 and 3 are nonlinear, linearization is applied and therefore the solution process must iterate (Mikhail *et al.*, 2001; Wang, 1990).

Each participant needs to be assigned a weight in the combined adjustment. In this study, the standard deviation of the image coordinates of the tie points is estimated as $\sigma_0 = 1$ pixel and assigned with unit weight. The weight factors for other observations and weighted parameters are calculated based on their *a priori* variances σ^2:

$$P = \frac{\sigma_0^2}{\sigma^2}. \qquad (5)$$

When compared to the tie points, the image coordinates of MOLA points receive smaller weights due to their large initial registration offset (approximately 30 pixels in image). For the MOLA ranges, they are introduced in the combined adjustment with a 10 m *a priori* standard deviation. As for the MOLA ground coordinates, they are considered as a quite accurate data source with *a priori* standard deviation of 10 m. The ground coordinates of tie points are virtually treated as free parameters, i.e., they receive infinitely small weight. Since the effects of sensor position and pointing to the bundle adjustment are highly correlated and their exact precision (especially the precision of pointing) is unclear, *a priori* standard deviation is chosen as 100 m or 200 m, respectively, for the nadir and off-nadir images with the sensor pointing precision matching the sensor position precision (1 arc minute is equivalent to approximately 100 meters on the ground at approximately 380 km altitude). Finally, it is noted that from past experience in photogrammetry and this study, the combined adjustment is not sensitive to the assignment of weight factors. Moderate changes in weight magnitude yield practically the same results.

Results and Evaluation

The combined adjustment will be evaluated in terms of exterior orientation refinement, ground position determination, and MOC and MOLA registration.

Refinement of Exterior Orientation

Since the exact correspondence of MOLA points on the MOC image cannot be measured at a high precision, the combined adjustment is mostly to use the geometry of MOC stereo images and MOLA ranges to refine the MGS trajectory data. Therefore, the refined exterior orientation is compared with the one obtained from the SPICE kernels. Table 2 and Figure 1 present their differences respectively in numeric and graphic forms. The horizontal axis of Figure 1 is the interval number, with one interval being 1/30 of the entire image. The results first reveal that Gusev Crater and Isidis Planitia receive mostly a constant correction in almost all exterior orientation elements because of the small magnitude of the RMSE compared to their corresponding mean values. Such constant correction varies from 1.9 m to 148.9 m in magnitude for sensor position, and from 0.14″ to 1′16″ for sensor pointing depending on the MOC images. Second, the much larger corrections in Eos Chasma suggest that the trajectory data may have noticeable uneven inconsistency from site to site. In this study, such inconsistency amounts to a maximum variation of 417.8 m in position and 20′ in pointing, which occurs in two images that were collected in a span of 48 days. It is noted that the two images in Eos Chasma belong to two different mapping extension phases. As a matter of fact, two different SPK and CK kernels were used to calculate the sensor positions and pointing for the left and right images in Eos Chasma, while the collection dates of the two images in Gusev Crater or Isidis Planitia refer to one

TABLE 2. DIFFERENCES BETWEEN SPICE AND REFINED EXTERIOR ORIENTATION (MEAN AND ROOT MEAN SQUARE ERRORS)

	Image		X(m)	Y(m)	Z(m)	ω	φ	κ
Eos Chasma	Left	Mean	13.288	−24.029	123.972	−4′ 5.13″	0′ 15.13″	0′ 25.07″
		RMSE	0.190	0.539	2.109	5′ 37.25″	0′ 38.65″	0′ 27.37″
	Right	Mean	0.756	22.347	−86.055	0′ 19.13″	0′ 5.93″	19′ 33.96″
		RMSE	35.027	110.955	417.77	0′ 57.15″	0′ 28.31″	20′ 35.68″
Gusev Crater	Left	Mean	−4.727	21.005	29.444	−0′ 3.20″	0′ 43.36″	0′ 18.74″
		RMSE	0.537	0.194	2.156	0′ 7.65″	0′ 3.68″	0′ 6.83″
	Right	Mean	24.715	−1.879	−148.94	0′ 34.05″	0′ 6.60″	−1′ 15.91″
		RMSE	0.477	0.253	1.784	0′ 3.91″	0′ 2.27″	0′ 4.14″
Isidis Planitia	Left	Mean	−5.817	28.040	−56.158	0′ 28.71″	0′ 1.49″	0′ −54.47″
		RMSE	0.292	0.196	2.294	0′ 0.14″	0′ 0.80″	0′ 0.38″
	Right	Mean	2.219	−6.830	56.878	0′ −24.13″	0′ −1.50″	0′ 21.35″
		RMSE	0.049	0.035	0.382	0′ 6.39″	0′ 0.47″	0′ 7.94″

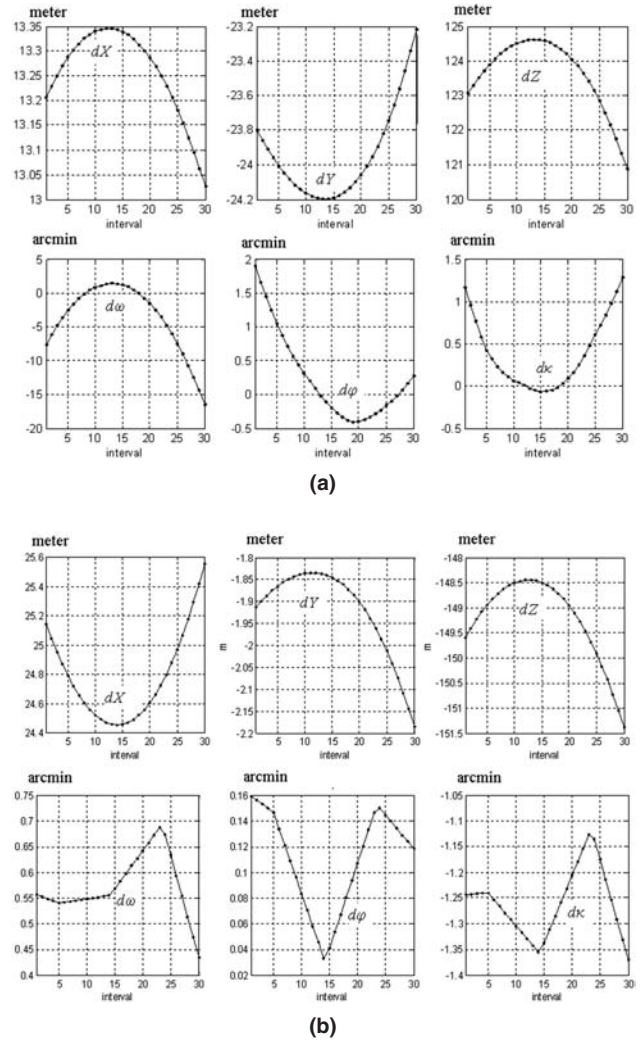

Figure 1. Differences between the SPICE and refined exterior orientations (horizontal axis: interval, being as 1/30 of the image; vertical axis: meter or arc minute): (a) Eos Chasma; (b) Gusev Crater.

SPK kernel and one CK kernel. The third observation compares the corrections of the two images in a stereo pair. The larger variance suggests that the trajectory data of the off-nadir image is much less consistent than the nadir image, which tends to have a constant correction in its exterior orientation elements. Our study justifies that the nadir and off-nadir trajectory data needs to receive different weights to achieve the best results for the combined adjustment. Finally, it needs to be pointed out that the corrections to sensor position are more systematic than the ones to sensor pointing. Figure 1 suggests apparent random errors in sensor pointing data.

TABLE 3. DIFFERENCES OF TIE POINT GROUND POSITION DETERMINED BY COMBINED ADJUSTMENT AND INTERSECTION USING SPICE KERNELS

Site		X(m)	Y(m)	Z(m)
Eos Chasma	Mean	−91.23	106.91	54.80
	RMSE	117.68	151.43	59.59
Gusev Crater	Mean	−1.79	0.37	6.75
	RMSE	2.72	0.34	1.07
Isidis Planitia	Mean	0.22	−1.79	3.07
	RMSE	0.16	0.99	2.72

Ground Position Determination

The ground position of a point can be determined in the combined adjustment (Mikhail *et al.*, 2001). Table 3 presents the differences of tie point ground positions determined by the combined adjustment and the intersection with the exterior orientation extracted from the SPICE kernels. For Gusev Crater and Isidis Planitia, the combined adjustment refines the intersection results to a magnitude of a few meters, with maximum 7.8 m (1 σ, approximately 2 pixels) in one coordinate component. However, the effect of the combined adjustment can be up to 257.3 m (1 σ) for Eos Chasma where the trajectory data is considerably refined. This concludes that the combined adjustment can strengthen the ground position solution through the geometry of the stereo pair, MOLA ranges and sensor modeling. Its benefit is significant when the trajectory data has large inconsistency. In the next section, we will further depict that the combined adjustment essentially provides both precise and correct ground positions by comparing them with the MOLA elevation profiles.

The precision of ground points can be theoretically estimated by using their covariance matrix. The *a posteriori* reference standard deviation $\hat{\sigma}_0$ is computed from the residuals of the measurements in the combined adjustment. The covariance matrix of the ground points is obtained by taking the inverse of the coefficient matrix of the normal equation systems as formulated in (Mikhail *et al.*, 2001). The results are summarized in Table 4. In all three study sites, the *a posteriori* reference standard deviations are very close to *a priori* ($\sigma_0 = 1$) reference standard deviation; the *a posteriori*

TABLE 4. ESTIMATED STANDARD DEVIATIONS OF MOLA AND TIE POINTS BY COMBINED ADJUSTMENT

Site	Type	$\hat{\sigma}_X$ (m)	$\hat{\sigma}_Y$ (m)	$\hat{\sigma}_Z$ (m)	$\hat{\sigma}_0$ (pixels)
Eos Chasma	MOLA	9.21	8.94	10.18	1.037
	Tie	99.01	141.64	43.30	
Gusev Crater	MOLA	7.87	10.21	10.16	1.059
	Tie	21.27	5.02	6.63	
Isidis Planitia	MOLA	9.84	7.33	9.85	1.014
	Tie	6.88	57.90	8.31	

standard deviations of the MOLA points are consistent with *a priori* estimation, 10 m. This suggests that all measurements and parameters are properly weighted in the combined adjustment and the theoretical estimation is reliable. The standard deviation of tie point determination is estimated as 178 m in 3D position in Eos Chasma, while for Gusev Crater and Isidis Planitia, it is 28 m and 59 m, respectively. This theoretical analysis is consistent with the exterior orientation refinement in Table 2 and the ground position corrections in Table 3. This suggests that the precision of ground position may vary from dozens of meters to over a hundred meters, depending on the quality of the trajectory data.

MOC and MOLA registration

MOC and MOLA registration can be used as a reliable, independent, and absolute quality measure for the combined adjustment. In this section, we examine the distribution of MOLA image coordinate corrections, and the overlay of MOLA elevation profiles with MOC images.

A correct combined adjustment should remove the known MOC and MOLA misregistration. This is essentially achieved by the refined MOC image orientation. Table 5 presents the statistics of the MOLA image coordinate corrections in the combined adjustment. As is shown, the average correction is from one to three dozen pixels in x (along track) image coordinate in all study sites, which suggests that the MOLA projections based on SPICE kernels are considerably changed along the flight direction. The small RMSE (<1 pixel) in Gusev Crater and Isidis Planitia indicates that the corrections in each of the two sites are nearly a constant. However, the Eos Chasma site presents a different property: their large RMSE suggests non-uniform or non-constant corrections over the images. This is consistent with the corrections to the trajectory data as presented earlier.

As a visual evaluation, Figure 2 plots the corrections of the image coordinates for Eos Chasma and Isidis Planitia. The size of the arrows represents the magnitude of the corrections; the left and right figures are respectively the central part of the left and right images of the stereo pairs. Points nearly in a straight line are the two MOLA profiles, while the tie points are randomly scattered. The ground distance between MOLA points and image pixel size listed in Table 1 can be used to estimate the dimension of the image. As shown in Figure 2, the MOLA points present much larger corrections than the tie points. The arrows of the tie points are not visible because of their small magnitude. Although the variation of MOLA image corrections is not noticeable in the shown limited portion of the images (approximately 12 to 20 MOLA points), their magnitude is considerably larger than the means listed in Table 5. Notice that the corrections are in opposite directions in the left and right images, which suggests the combined adjustment balances the inconsistency in the trajectory data.

Finally, the MOLA points and their topographic heights are overlaid with the MOC images. As shown in Figure 3, all three study sites present significant registration improvement compared to the results before the combined adjustment (Shan *et al.*, 2005). For example, the MOLA point with the index number 77 in Gusev Crater is projected to the same location slightly outside the crater on both images. All results in Figure 3 reveal that the combined adjustment can correct the misregistration, and consequently, the MOC images are precisely registered to the same MOLA points on the ground. To further evaluate the correctness of the combined adjustment, Figure 4 plots the MOLA topographic heights next to the MOC images. The right edge of the image

TABLE 5. MOLA IMAGE COORDINATE CORRECTIONS IN COMBINED ADJUSTMENT

		Left (pixels)		Right (pixels)	
Site		x	y	x	y
Eos Chasma	Mean	12.79	4.04	−8.42	47.10
	RMSE	61.72	15.92	−18.12	40.52
Gusev Crater	Mean	−24.18	3.29	24.90	−2.70
	RMSE	0.77	0.25	0.10	0.16
Isidis Planitia	Mean	35.04	−2.71	−24.79	2.89
	RMSE	0.08	0.20	1.52	0.36

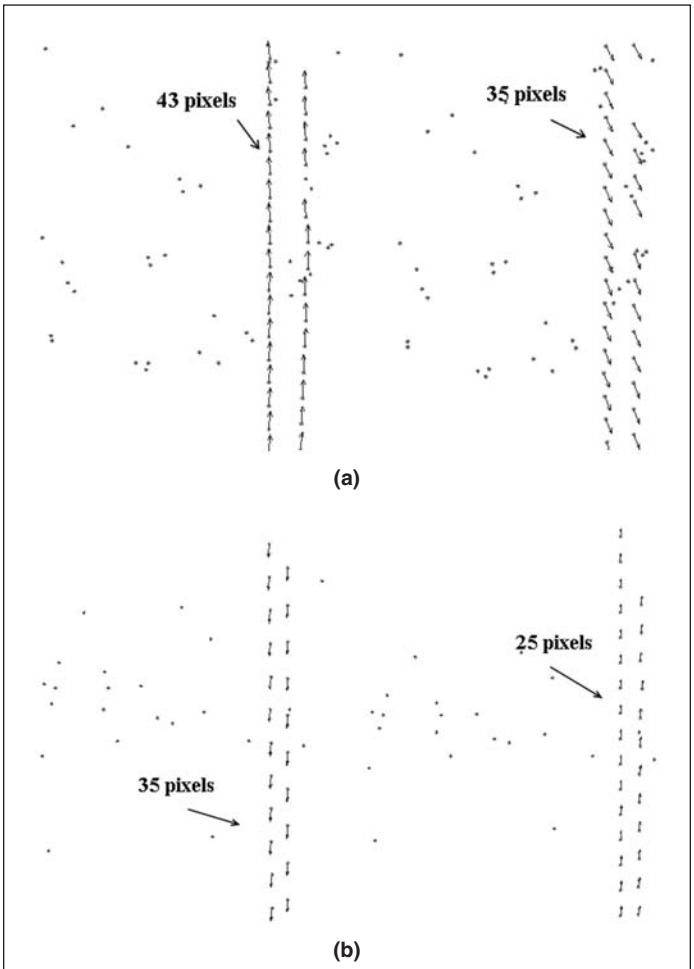

Figure 2. Image coordinate corrections of MOLA and tie points (Middle portion of the images. Top: Eos Chasma; Bottom: Isidis Planitia. Individual dots are tie points, and dots with arrows are MOLA points.).

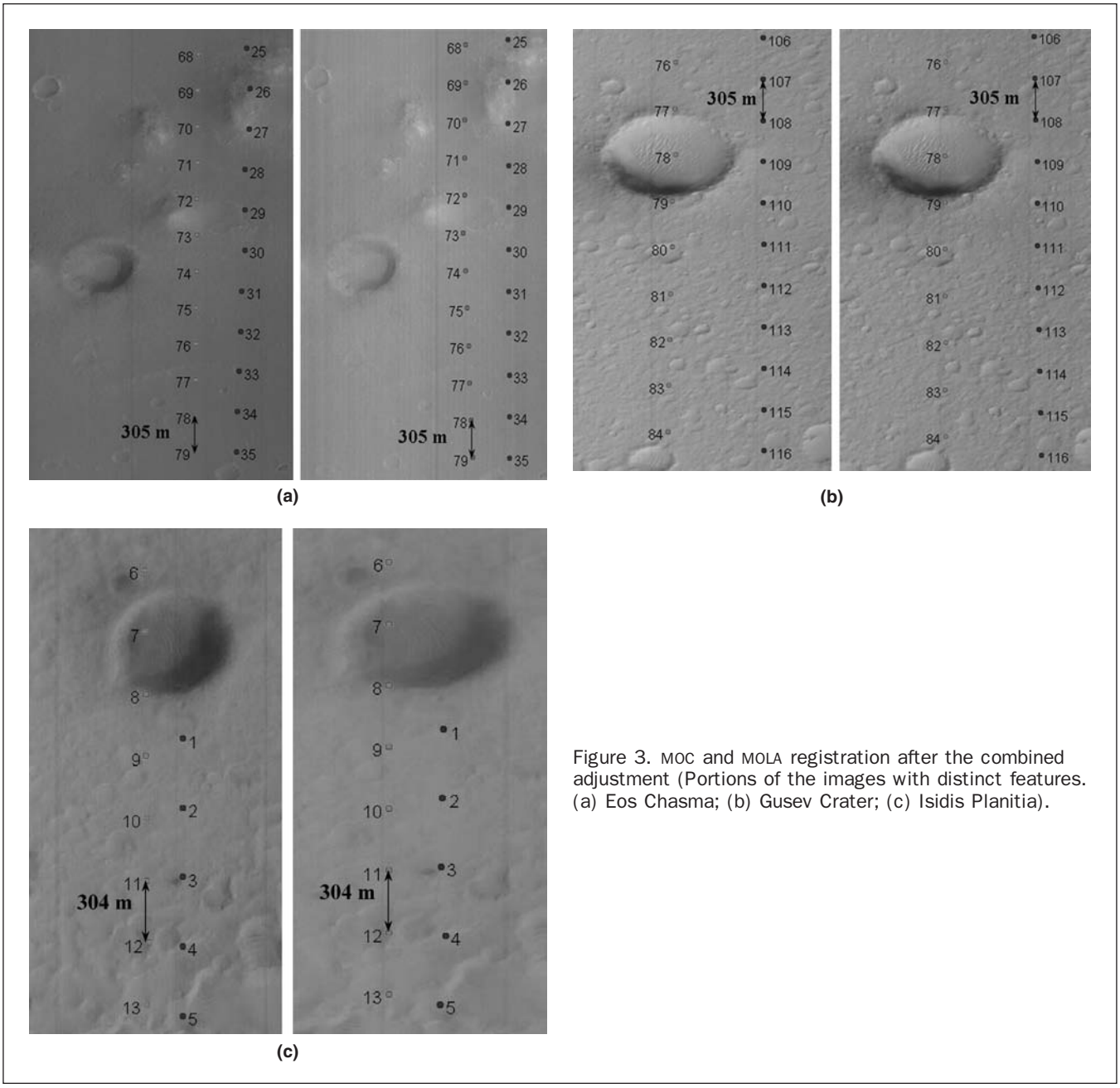

Figure 3. MOC and MOLA registration after the combined adjustment (Portions of the images with distinct features. (a) Eos Chasma; (b) Gusev Crater; (c) Isidis Planitia).

is used as the height reference and the horizontal distance from the edge to the MOLA points (*symbols in Figure 4) represents the topographic height. Presented in Figure 4 are locations where noticeable topographic relief exits in the three study sites. As is shown, the MOLA points inside a crater have lower topographic height than the MOLA points in the neighborhood. Based on the above evaluation, it can therefore conclude that the combined adjustment yields a precise and correct MOC-MOLA registration.

Conclusions

The proposed combined adjustment provides a mathematical model for integrated MGS mapping data processing. In this model, both observations and parameters are weighted according to their *a priori* statistical properties such that it is convenient to include various types of mapping data and balance their effects in the combined adjustment. In addition to MOC images, trajectory data, MOLA ranges, and MOLA points used in this study, this model can be further expanded to include other data such as MOLA DEM.

The study reveals that inconsistency may exist in the trajectory data, of which sensor pointing presents larger irregular variation than sensor position. The combined adjustment considerably refines the trajectory data, including both sensor position and sensor pointing. In this process, the primary contributors are MOC stereo image as well as MOLA ranges and MOLA ground points. As a result of the combined adjustment, the intersection positions calculated by directly using the trajectory data are refined by an amount from several meters to over 257 meters, depending on the quality of the trajectory data.

Registering the MOLA topographic profiles to MOC stereo images provides an independent, absolute and reliable evaluation for the combined adjustment. It is shown that the large misregistration between MOC and MOLA can be corrected

(a)

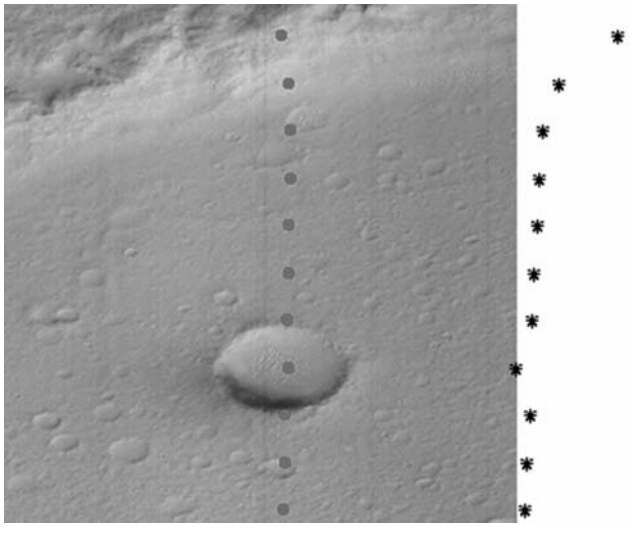

(b)

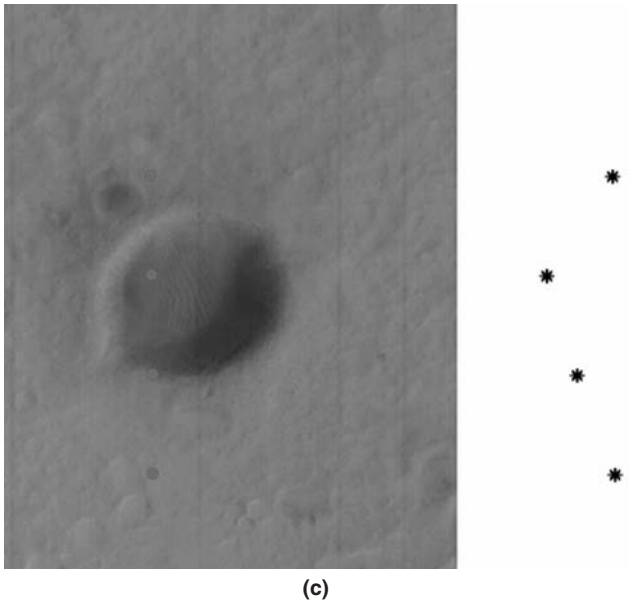

(c)

Figure 4. MOLA topographic profile overlaid with MOC image (Portions of the images with distinct relief. (a) Eos Chasma, top section of the image; (b) Gusev Crater, bottom section of the image; (c) Isidis Planitia, top section of the image).

by the combined adjustment. The final MOC and MOLA overlay precisely follows the MOLA topographic relief. Theoretical estimation shows that the precision of ground point determination with the combined adjustment varies from 28 to 178 meters, depending on the quality of the trajectory data.

Mars topographic data processing deserves a continuous effort. Using up-to-date refined SPICE kernels and MOLA data will likely further improve the combined adjustment results. Tests over areas covered by a larger number of images are also of interest. This would help further confirm the large pointing inconsistency found in this study and investigate the properties of the trajectory data over different mission phases.

Acknowledgments

This study is supported by NASA. Helpful for this study were inputs from, and discussions with Randolph Kirk at the U.S. Geological Survey, Gregory Neumann at the Massachusetts Institute of Technology, and Charles Acton at the Jet Propulsion Laboratory. The critical comments and suggestions from anonymous reviewers improved the manuscript by including related studies and clarifying several ambiguities.

References

Abshire, J.B., X. Sun, and R.S. Afzal, 2000. Mars Orbiter Laser Altimeter: receiver model and performance analysis, *Applied Optics*, Vol. 39, pp. 2440–2460.

Acton, C., 1996. Ancillary data services of NASA's navigation and ancillary information facility, *Planetary and Space Science*, 44, pp. 65–70.

Albee, A.L., R.E. Arvidson, F. Palluconi, and T. Thorpe, 2001. Overview of the Mars Global Surveyor mission, *Journal of Geophysical Research*, Vol. 106, No. E10, pp. 23291–23316.

Albertz, J., M. Attwenger, J. Barrett, S. Casley, P. Dorninger, E. Dorrer, H. Ebner, S. Gehrke, B. Giese, K. Gwinner, C. Heipke, E. Howington-Kraus, R.L. Kirk, H. Lehmann, H. Mayer, J-P. Muller, J. Oberst, A. Ostrovskiy, J. Renter, S. Reznik, R. Schmidt, F. Scholten, M. Spiegel, U. Stilla, M. Wählisch, G. Neukum and the HRSC Col-Team, 2005. HRSC on Mars Express – Photogrammetric and Cartographic Research, *Photogrammetric Engineering & Remote Sensing*, 71(10).

Anderson, F.S., and T.J. Parker, 2002. Characterization of MER landing sites using MOC and MOLA, *The 33rd Lunar and Planetary Science Conference*, 11–15 March, League City, Texas.

Archinal, B.A., E.M. Lee, R.L. Kirk, T.C. Duxbury, R.M. Sucharski, D.A. Cook, and J.M. Barrett, 2004. MDIM 2.1: A geodetically precise global Viking image mosaic of Mars based on MOLA control, *International Archives of Photogrammetry and Remote Sensing*, XXXV, B, "Geo-Imagery Bridging Continents", Istanbul, unpaginated DVD-ROM.

Caplinger, M., 2003. Mass production of DEMs from MOC stereopairs, ISPRS-ET Working Group IV/9 Workshop "Advances in Planetary Mapping 2003", URL: *http://astrogeology.usgs.gov/Projects/ISPRS/MEETINGS/Houston2003/abstracts/Caplinger_isprs_mar03.pdf* (last date accessed: 13 July 2005).

Duxbury, T.C., R.L. Kirk, B.A. Archinal, and G.A. Neumann, 2002. Mars Geodesy/Cartography Working Group recommendations on Mars cartographic constants and coordinate systems. *International Archives Photogrammetry and Remote Sensing*, XXXIV(4), "Geospatial Theory, Processing and Applications", Ottawa, unpaginated CD-ROM.

Ebner, H., M. Spiegel, A. Baumgartner, B. Giese, and G. Neukum, 2004. Improving the Exterior Orientation of Mars Express HRSC Imagery, *International Archives of Photogrammetry and Remote Sensing*, XXXV, B, "Geo-Imagery Bridging Continents", Istanbul, unpaginated DVD-ROM.

Ivanov, A.B., 2003. Ten-Meter Scale Topography and Roughness of Mars Exploration Rovers Landing Sites and Martian Polar Regions, The 34th Lunar and Planetary Science Conference, 17–21 March, League City, Texas, URL: *http://www.lpi.usra.edu/meetings/lpsc2003/pdf/2084.pdf* (last date accessed: 13 July 2005).

Kirk, R.L., L.A. Soderblom, E. Howington-Kraus, and B. Archinal, 2002. USGS high resolution topomapping of Mars with Mars

Orbiter Camera Narrow-angle Images, *International Archives of Photogrammetry and Remote Sensing*, Vol.34, Part 4, "GeoSpatial Theory, Processing and Applications", Ottawa, unpaginated CD-ROM.

Kirk, R.L., E. Howington-Kraus, B. Redding, D. Galuszka, T.M. Hare, B.A. Archinal, L.A. Soderblom, and J.M. Barrett, 2003. High-resolution topomapping of candidate MER landing sites with Mars Orbiter Camera Narrow-Angle images, *Journal of Geophysical Research*, 108 (E12), 8088, (doi:10.1029/2003JE002131).

Kirk, R.L., E. Howington-Kraus, T. Hare, R. Soricone, K. Ross, L. Weller, M. Rosiek, B. Redding, D. Galuszka, and B.A. Archinal, 2004. High-resolution topomapping of Mars: Life after MER site selection, *Lunar and Planetary Science*, XXXV, Abstract 2046, Lunar and Planetary Institute, Houston, unpaginated CD-ROM.

Malin, M.C., and S.K. Edgett, 2001. Mars Global Surveyor Orbiter Camera: Interplanetary cruise through primary mission, *Journal of Geophysical Research*, Vol. 106, No. E10, 25 October, pp. 23429–23570.

Mikhail, E.M., J.S. Bethel, J.C. McGlone, 2001. *Introduction to Modern Photogrammetry*, John Wiley & Sons, Inc., 479 pages.

Neumann, G., F. Lemoine, D. Rowlands, D.E. Smith, and M.T. Zuber, 2001. Crossover analysis in MOLA data processing, *Journal of Geophysical Research*, Vol. 106, No. E10, pp. 23753–23768.

Parker, T., M. Malin, M. Golombek1, T. Duxbury, A. Johnson, J. Guinn1, T. McElrath, R. Kirk, B. Archinal, L. Soderblom, R. Li, and the MER Navigation Team and Athena Science Team, 2004. Location, Location, Location, Lunar and Planetary Science 35, URL: *http://www.lpi.usra.edu/meetings/lpsc2004/pdf/2189.pdf* (last day accessed: 13 July 2005).

Rosiek, M.R., R. Kirk, T. Hare, and E. Howington-Kraus, 2001. Utilizing Mars Digital Image Model (MDIM) and Mars Orbiter Laser Altimeter (MOLA) data for photogrammetry control, ISPRS Working Group IV/9 Workshop "Planetary Mapping 2001", URL: *http://astrogeology.usgs.gov/Projects/ISPRS/Meetings/Flagstaff2001/abstracts/isprs_etm_OCT01_rosiek_mars_photogrammetry.pdf* (last day accessed 13 July 2005).

Rosiek, M.R., R.L. Kirk, B.A. Archinal, E. Howington-Kraus, T. Hare, D. Galuszka, and B. Redding, 2005. Utility of Viking Orbiter images and products for Mars mapping, *Photogrammetric Engineering & Remote Sensing*, 71(10).

Seidelmann, P.K., V.K. Abalakin, M. Bursa, M.E. Davies, C. de Bergh, J.H. Lieske, J. Oberst, J.-L. Simon, E.M. Standish, P. Stooke, P.C. Thomas: 2002, Report of the IAU/IAG working group on cartographic coordinates and rotational elements of the planets and satellites: 2000, *Celestial Mechanics and Dynamical Astronomy*, Vol. 82, No. 1, pp. 83–110.

Shan, J., J-S Yoon, D.S. Lee, R.L. Kirk, G. A. Neumann and C.H. Acton, 2005. Photogrammetric analysis of the Mars Global Surveyor mapping data, *Photogrammetric Engineering & Remote Sensing*, (71), 1:97–108.

Slavney, S., and R.E. Arvidson, 2000, MOLA Standard Product Archive Volume Software Interface Specification (MOLA Archive Volume SIS), Washington University, St. Louis, Missouri.

Smith, D.E., M.T. Zuber, H.V. Frey, J.B. Garvin, J.W. Head, D.O. Muhleman, G.H. Pettengill, R.J. Phillips, S. Solomon, H.J. Zwally, W.B. Banerdt, T.C. Duxbury, M.P. Golombek, F.G. Lemoine, G.A. Neumann, D.D. Rowlands, O. Aharonson, P.G. Ford, A.B. Ivanov, C.L. Johnson, P.J. McGovern, J.B. Abshire, R.S. Afzal, and X. Sun, 2001. Mars Orbiter Laser Altimeter: Experiment summary after the first year of global mapping of Mars, *Journal of Geophysical Research*, Vol. 106, No. E10, pp. 23689–23722.

Wang, Z.Z., 1990. *Principles of Photogrammetry (with Remote Sensing)*, Press of Wuhan Technical University of Surveying and Mapping, Publishing House of Surveying and Mapping, Beijing, 575 pages.